

Chemical Potential Diagrams for La-M-Zr-O (M=V, Cr, Mn, Fe, Co, Ni) Systems : Reactivity of Perovskites with Zirconia as a Function of Oxygen Potential

Harumi YOKOKAWA*, Natsuko SAKAI, Tatsuya KAWADA
and Masayuki DOKIYA

Received January 10, 1990 ; Accepted April 20, 1990

The chemical potential diagrams for the La-M-Zr-O (M=transition metals) systems at 1273 K have been constructed as a $\log P(O_2)$ vs. $\log \{a(M)/a(La)\}$ plot under a condition of $a(ZrO_2)=1$. Since only a $La_2Zr_2O_7$ phase is known as double oxides in the La-Zr-O system, the thermodynamic features of reactions of perovskites, $LaMO_3$, with ZrO_2 can be judged in terms of whether or not $La_2Zr_2O_7$ is formed. To simultaneously present stability of perovskites against decompositions as well as their compatibility with ZrO_2 , the chemical potential diagrams for the La-M-O systems have been superimposed on those for the La-Zr-M-O systems drawn using the same coordinates; in the combined diagram, areas of those compounds which react with ZrO_2 to form $La_2Zr_2O_7$ are completely covered by the stability polygon of $La_2Zr_2O_7$.

1. INTRODUCTION

There has been a growing interest in applying sophisticated thermodynamic analyses to practical materials problems.¹⁻³⁾ While chemical equilibria calculations⁴⁻⁶⁾ and phase diagram calculations^{7,8)} have been successfully extended to multicomponent systems, few attempts have been made so far to construct chemical potential diagrams for multicomponent systems except for the geochemical fields.^{9,10)}

We have engaged in making chemical thermodynamic considerations on materials problems in energy-related fields. In due course, we established a thermodynamic database for inorganic compounds and combined it with the SOLGAS-

MIX program for calculating chemical equilibria.^{4,6)} To facilitate further applications of such a database, we wrote a computer program, CHD,^{11,12)} for constructing chemical potential diagrams. Since a simple but generalized algorithm was adopted, it is quite easy to construct chemical potential diagrams for multicomponent systems. In particular, the multicomponent systems having two metallic elements (M1 and M2) can be treated without any difficulty so that chemical potential diagrams for M1-M2-O¹³⁾, M1-M2-C-O¹⁴⁾, M1-M2-H-O-e¹⁵⁾ and M1-M2-H¹⁶⁾ systems have been successfully constructed and analyzed from the materials chemistry viewpoint. In the present study, this attempt has been further extended to construct diagrams for the multicomponent systems having more than two metallic elements; as an example, we selected the La-M-Zr-O (M=transition metal) systems of technological importance in developing a solid oxide fuel cell.

Materials Chemistry Division, National Chemical Laboratory for Industry, Tsukuba research center, Ibaraki 305 Japan

Keywords : Chemical potential diagram,
Stability, Reactivity,
Perovskite, Zirconia

2. PEROVSKITE MATERIALS IN A SOLID OXIDE FUEL CELL

A solid oxide fuel cell consists mainly of ceramic materials such as YSZ (Yttria Stabilized Zirconia) electrolyte, LaMnO₃-based air electrode, Ni/YSZ cermet fuel electrode and LaCrO₃-based separator.¹⁷⁻¹⁹⁾ The chemical compatibility among these materials becomes quite important during a high-temperature (>1500 K) fabricating process and also during a long-term operation around 1300 K. In our previous investigations,²⁰⁻²²⁾ the general chemical features of reactions between perovskites and ZrO₂ have been derived as follows: Although unusually high valence states of transition metal ions such as Fe⁴⁺ and Cu³⁺ may be stabilized in the perovskite-type crystal structure, those perovskites tend to react with ZrO₂ to form a transition metal compound containing lower valence states.²⁰⁾

In the present study, the thermodynamic features of reactions between transition metal perovskites and ZrO₂ are reexamined as a function of oxygen partial pressure with an emphasis on interrelationship between the chemical and the geometrical features in chemical potential diagrams.

3. CONSTRUCTION OF CHEMICAL POTENTIAL DIAGRAMS

The pyrochlore phase, La₂Zr₂O₇, is known as one of reaction products.²³⁻²⁵⁾ In the absence of other zirconium compounds in the La-Zr-M-O system, the thermodynamic features of reactions of LaMO₃ with ZrO₂ can be examined in terms of whether or not La₂Zr₂O₇ is formed. This is common to almost all LaMO₃ (M=V,Cr,Mn,Fe,Co,Ni); only one exception is the formation of La₂NiZrO₆ phase in a reaction between La₂NiO₄ and ZrO₂.²⁶⁾ Thus, the present chemical potential diagrams for the La-M-Zr-O systems have been constructed in the following way;

1) First, one diagram is constructed for

the La-M-O system in a log P(O₂) vs. log {a(M)/a(La)} plot. In this plot, compounds are represented as polygons; their horizontal width shows the stability of the compound as a function of oxygen potentials, whereas the vertical width represents the stability of the double oxide from their constituent oxides. The slope of borderlines depends on stoichiometry or valence number of two phases.¹³⁾

2) another diagram for the La-Zr-M-O {a(ZrO₂)=1} system is constructed using the same coordinates and then superimposed on the chemical potential diagram obtained above.

In such combined diagrams, those compounds which can stably coexist with ZrO₂ appear without change, whereas the stability areas of those compounds which should react with ZrO₂ are completely covered by that of La₂Zr₂O₇; these are presented as dashed lines in the present diagrams.

The thermodynamic data used to construct the present diagrams were already reported elsewhere.²⁰⁻²²⁾

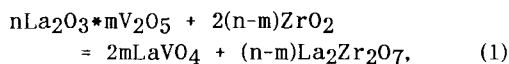
3.1 La-Zr-V-O system

In the La-V-O system, five double oxides are known; that is, LaVO₃, LaVO₄, and nLa₂O₃·mV₂O₅ (n/m = 1.62/0.38, 3/1, 1.42/0.58). The last four double oxides have the pentavalent vanadium ions; in the chemical potential diagram shown in Fig. 1, these four compounds appear sequentially between V₂O₅ and La₂O₃. LaVO₃ appears between V₂O₃ and La₂O₃. The difference in slope between V₂O₃/LaVO₃/La₂O₃ borderlines and V₂O₅/LaVO₄/La₂O₃ borderlines is due to the difference of the valence state of vanadium ions.

When zirconium is added and the activity of ZrO₂ is fixed at unity, the lower part of the chemical potential diagram is changed; that is, instead of La₂O₃, La₂Zr₂O₇ appears. Its area is larger than that of La₂O₃. Correspondingly, some polygons disappear and some lose partially their own area. These changes

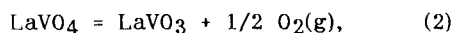
in the diagram can be related with chemical reactions as follows.

The stability areas of $n\text{La}_2\text{O}_3 \cdot m\text{V}_2\text{O}_5$ are completely covered by that of $\text{La}_2\text{Zr}_2\text{O}_7$. This means that $n\text{La}_2\text{O}_3 \cdot m\text{V}_2\text{O}_5$ tend to react with ZrO_2 . These chemical reactions can be written as follows;

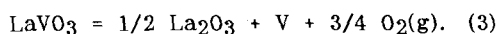


in which the valence state of vanadium ions does not change. Thus, these reactions can be characterized as the recombination of constituent oxides which may be caused by the difference in the stabilization energy from constituent oxides among $\text{La}_2\text{Zr}_2\text{O}_7$, LaVO_4 and $n\text{La}_2\text{O}_3 \cdot m\text{V}_2\text{O}_5$.

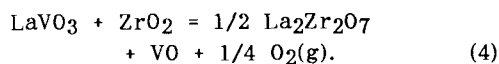
Note that the polygon of $\text{La}_2\text{Zr}_2\text{O}_7$ partially covers those of LaVO_3 and LaVO_4 , indicating that LaVO_4 and LaVO_3 can coexist with both ZrO_2 and $\text{La}_2\text{Zr}_2\text{O}_7$. The equilibrium oxygen partial pressure between LaVO_3 and LaVO_4 is derived from the following reaction;



which is not affected by the presence of ZrO_2 nor of $\text{La}_2\text{Zr}_2\text{O}_7$. On the other hand, the decomposition oxygen partial pressure of LaVO_3 is affected by the presence of ZrO_2 . In the absence of ZrO_2 , LaVO_3 decomposes as follows;



In the presence of ZrO_2 , LaVO_3 decomposes as follows;



Since the main reaction product changes from La_2O_3 to $\text{La}_2\text{Zr}_2\text{O}_7$, the decomposition oxygen partial pressure increases, and the decomposition product of the vanadium component changes from V metal in eq. (3) to $\text{VO}(\text{s})$ in eq. (4). The present diagram clearly shows why reaction products as well as the decomposition pressure change in the presence of ZrO_2 .

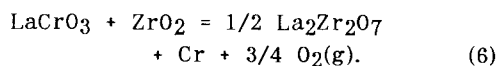
3.2 La-Zr-Cr-O system

In the present treatment, lanthanum chromates, namely, La_2CrO_6 and its decomposition derivatives²⁷⁾, are neglected; this is partly because no experimental value nor estimate is available at present for their thermodynamic properties. Since behavior of these compounds may become important in preparing LaCrO_3 -based interconnectors in a planar solid oxide fuel cell, it is hoped to construct diagrams including these compounds.

The present chemical potential diagram without lanthanum chromates is simple (see Fig. 2). The stability polygon of LaCrO_3 is wide and it decomposes only in an extremely reductive atmosphere;



LaCrO_3 does not react with ZrO_2 except for an extremely reductive condition as follows;

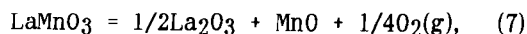


In a practical sense, it can be concluded that LaCrO_3 and ZrO_2 is chemically compatible. This is apparently due to the fact that the stabilization energy of LaCrO_3 from La_2O_3 and Cr_2O_3 (estimated as -34×2 kJ/mol) is much larger than that of $\text{La}_2\text{Zr}_2\text{O}_7$ (evaluated as -22×4 kJ/mol).

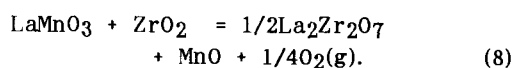
Although chromates are excluded in the present treatment, their possible effects can be qualitatively predicted from comparison with the La-Zr-V-O system; that is, La_2CrO_6 will appear at the lower and right-hand side of the polygon of LaCrO_3 and will be covered partly by the polygon of $\text{La}_2\text{Zr}_2\text{O}_7$.

3.3 La-Zr-Mn-O system

LaMnO_3 decomposes as follows;



whereas LaMnO_3 reacts with ZrO_2 in a reductive atmosphere as follows;



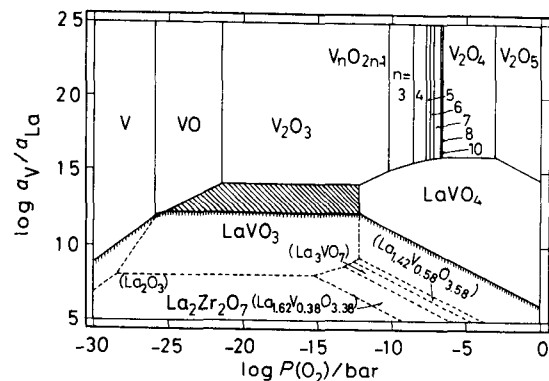


Fig. 1 Chemical potential diagram for La-Zr-V-O system at 1273 K under a condition of $a(\text{ZrO}_2)=1$; dotted lines show the stability polygons of double oxides in La-V-O system. Superimposed area of $\text{La}_2\text{Zr}_2\text{O}_7$ indicates that $n\text{La}_2\text{O}_3 \cdot m\text{V}_2\text{O}_5$ phases react with ZrO_2 to decompose into $\text{La}_2\text{Zr}_2\text{O}_7$ and LaVO_4 .

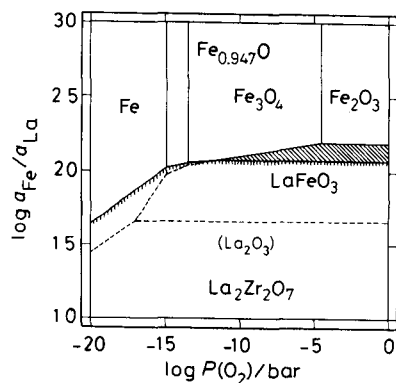


Fig. 4 Chemical potential diagram for La-Zr-Fe-O system at 1273 K under a condition of $a(\text{ZrO}_2)=1$.

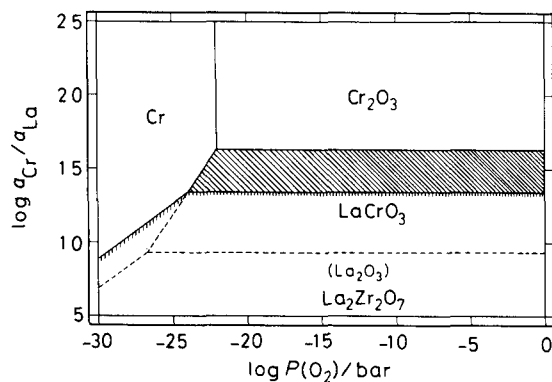


Fig. 2 Chemical potential diagram for La-Zr-Cr-O system at 1273 K under a condition of $a(\text{ZrO}_2)=1$.

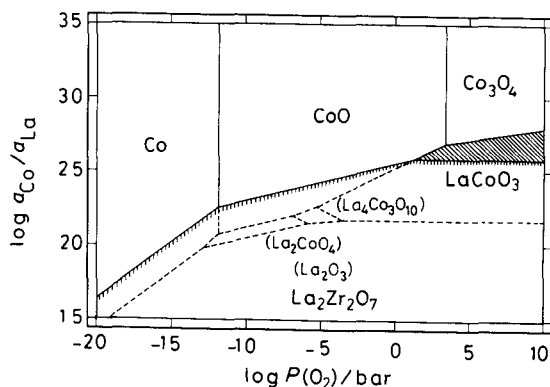


Fig. 5 Chemical potential diagram for La-Zr-Co-O system at 1273 K under a condition of $a(\text{ZrO}_2)=1$. $\text{La}_4\text{Co}_3\text{O}_{10}$ and La_2CoO_4 react with ZrO_2 .

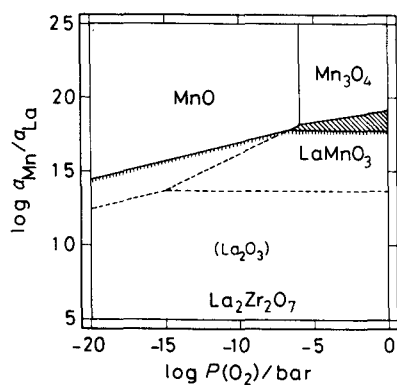


Fig. 3 Chemical potential diagram for La-Zr-Mn-O system at 1273 K under a condition of $a(\text{ZrO}_2)=1$.

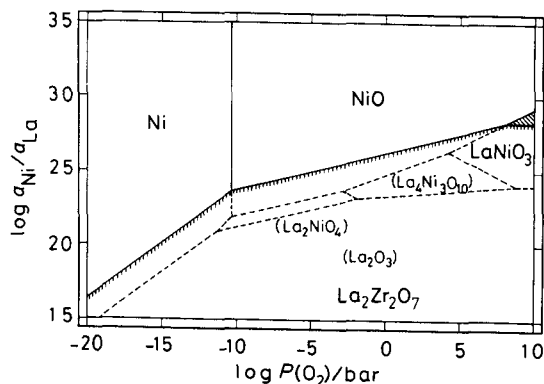


Fig. 6 Chemical potential diagram for La-Zr-Ni-O system at 1273 K under a condition of $a(\text{ZrO}_2)=1$. LaNiO_3 is not stable in air. $\text{La}_4\text{Ni}_3\text{O}_{10}$ and La_2NiO_4 are not stable against reactions with ZrO_2 .

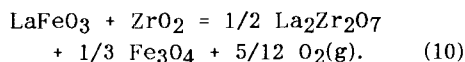
The decomposition oxygen pressure for eq. (7) is about 10^{-15} bar at 1273 K, whereas the equilibrium oxygen pressure for eq. (8) is about 10^{-6} bar. This change in oxygen pressure caused by the presence of ZrO_2 is larger in the La-Zr-Mn-O system than in the La-Zr-Cr-O system. This is due to the difference in the chemical reaction scheme given in eqs. (5)-(8). In the La-Zr-Cr-O system, one of reaction products is Cr, whereas MnO is formed in the La-Zr-Mn-O system; correspondingly, the mole number of evolved oxygen per one mole of transition metal in eq. (6) is three times larger than that in eq. (8). When the valence change of the transition metal on reaction is large, the effect of the presence of ZrO_2 becomes small. Interrelation between these chemical features and the geometrical features in the chemical potential diagram will be discussed later from the thermodynamic point of view.

3.4 La-Zr-Fe-O system

Although $LaFeO_3$ decomposes into La_2O_3 and Fe,



the decomposition reaction in the presence of ZrO_2 can be written as follows;

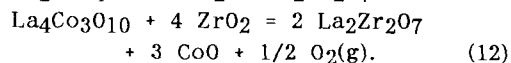
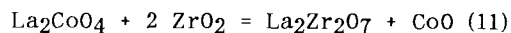


The decomposition product is Fe_3O_4 instead of Fe in eq. (9), and the equilibrium oxygen pressure is shifted to the oxidative side as given in Fig. 4. These features are similar to those of $LaVO_3$.

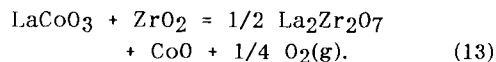
3.5 La-Zr-Co-O system

In the La-Co-O system, $LaCoO_3$, $La_4Co_3O_{10}$ and La_2CoO_4 are known. Figure 5 shows that the stability areas of La_2CoO_4 and of $La_4Co_3O_{10}$ are located in a limited region of oxygen partial pressure and are both covered by $La_2Zr_2O_7$; this suggests that these compounds are not compatible with ZrO_2

as follows;



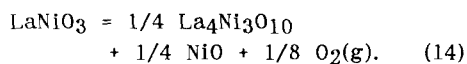
$LaCoO_3$ reacts with ZrO_2 to form $La_2Zr_2O_7$ even in air at 1273 K.



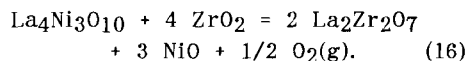
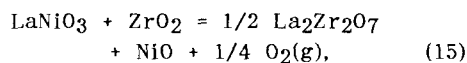
Note that the stability area of $LaCoO_3$ is mainly delimited by CoO in the upper side of the diagram; this makes the stability area of $LaCoO_3$ sharpened to the reductive side and also gives rise to a large shift of the equilibrium oxygen partial pressure to the oxidative side in the presence of ZrO_2 .

3.6 La-Zr-Ni-O system

At 1273 K, $LaNiO_3$ is no more stable in air against decompositions as shown in Fig. 6. $LaNiO_3$ decomposes as follows;



$La_4Ni_3O_{10}$ as well as $LaNiO_3$ react with ZrO_2 as follows;



The formation of La_2ZrNiO_6 ²⁶⁾ will be discussed later.

3.7 Effects of Temperature in La-Zr-Mn-O system

Since a good electrical contact between electrode and electrolyte can be obtained by high temperature heat treatment, it is of technological importance to see whether or not the reaction between two materials proceeds at high temperatures. Figure 7 shows the chemical potential diagrams for the La-Zr-Mn-O system at selected temperatures. Since the reaction between $LaMnO_3$ and ZrO_2 given in eq. (8) is accompanied with the reduction of transition metal ions, the equilibrium oxygen partial pressure increases with increasing temperature.

Correspondingly, the reductive-side corner of the hatched area of LaMnO_3 moves to the oxidative side with increasing temperature.

4. NONSTOICHIOMETRY OF LaMnO_3

LaMnO_3 is the perovskite compound that has the most appreciable A-site nonstoichiometry among the transition metal perovskites.^{28,29)}

We have made an attempt¹⁹⁾ to represent the nonstoichiometric LaMnO_3 in terms of an ideal association solution consisting of $\text{La}_{0.667}\text{MnO}_3$, $\text{La}_{0.667}\text{MnO}_{2.5}$, LaMnO_3 and $\text{LaMnO}_{2.5}$. After their thermodynamic parameters were determined so as to reproduce the thermogravimetric results, the stable composition region of $\text{La}_y\text{MnO}_{3-\delta}$ and its reaction zone with Y_2O_3 stabilized ZrO_2 (YSZ) were calculated as functions of oxygen partial pressure and temperature using the CTC/SOLGASMIX program.^{4,6)}

In Fig. 8, results of chemical equilibria calculations at 1273 K are reproduced at the upper part, whereas at the lower part, the same equilibria are plotted in the present adopted chemical potential diagram; note that in this calculations, YSZ was adopted as one of reactants. For comparison, phase equilibria obtained without consideration on nonstoichiometry are also presented as dashed lines. To directly compare with results for YSZ in which the activity of ZrO_2 is about 0.6, dotted and dashed lines were obtained for the case of $a(\text{ZrO}_2) = 0.6$.

Figure 8 shows that the stability polygon of LaMnO_3 can be divided into the hatched ZrO_2 -compatible area and the $\text{La}_2\text{Zr}_2\text{O}_7$ -compatible area. An important point is that this feature in chemical potentials actually corresponds to the reaction between perovskites and ZrO_2 ; that is, the manganites in the $\text{La}_2\text{Zr}_2\text{O}_7$ -compatible area can react with ZrO_2 to form $\text{La}_2\text{Zr}_2\text{O}_7$ and the La-poorer manganites. Note that this reaction can take place even in air; in this sense,

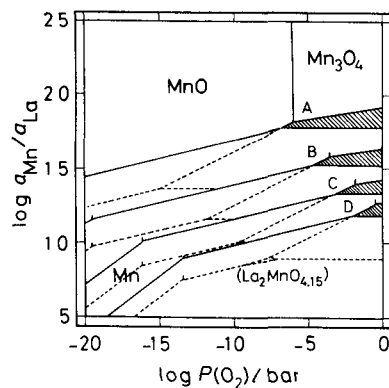


Fig. 7 Effect of temperature on phase relations in La-Zr-Mn-O system under a condition of $a(\text{ZrO}_2)=1$. A = 1273 K; B = 1473 K; C = 1673 K; D = 1873 K. The K_2NiF_4 compound, $\text{La}_2\text{MnO}_{4.15}$, appears at high temperatures.

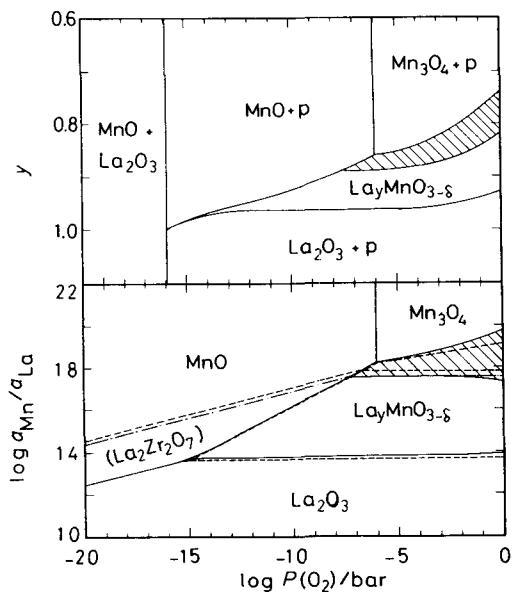


Fig. 8 Effect of nonstoichiometry in $\text{La}_y\text{MnO}_{3-\delta}$. The upper diagram indicates the stable region of La stoichiometry, y , in $\text{La}_y\text{MnO}_{3-\delta}$ as a function of oxygen partial pressure, $\log P(\text{O}_2)/\text{bar}$. The lower is the chemical potential diagrams with and without treatment of La nonstoichiometry.

this reaction is different from those represented by eqs. (4) and (8).

Since the stability polygons of perovskites are all divided in terms of the compatibility with ZrO_2 as shown in Figs. 1 to 6, this implies that if there would be small La nonstoichiometry in other perovskites (for example, $LaCrO_3$), the perovskites in the La-rich side can react with ZrO_2 to form $La_2Zr_2O_7$ and the La-poorer perovskites.

5. DISCUSSION

The reaction of transition metal perovskites with ZrO_2 can be characterized as a combination of the $La_2Zr_2O_7$ formation and the reduction of transition metal ions.²⁰ The former $La_2Zr_2O_7$ formation is common to all system, whereas the latter reduction depends on system. In this section, interrelationship will be examined between these chemical features and the geometrical features in the chemical potential diagram; a special emphasis will be placed on effects of the valence state of transition metals on the chemical features of the reactions.

The $La_2Zr_2O_7$ formation as a result of reaction between perovskites and ZrO_2 is represented by the point that stability polygons of perovskites are narrowed by the polygon of $La_2Zr_2O_7$ instead of La_2O_3 . Since two borderlines between $LaMO_3$ and La_2O_3 and between $LaMO_3$ and $La_2Zr_2O_7$ are both horizontal, it is easy to compare the extent of shift among Figs. 1 to 6. The same magnitude of shift can be explained thermodynamically as follows:

The borderline between $LaMO_3$ and La_2O_3 is represented by the following chemical potentials of compounds;

$$\begin{aligned} \mu(La) + \mu(M) + 3\mu(O) &= \Delta_f G^\circ(LaMO_3), \quad (17) \\ 2\mu(La) + 3\mu(O) &= \Delta_f G^\circ(La_2O_3). \quad (18) \end{aligned}$$

Since the vertical axis variable is given as $\log \{a(M)/a(La)\} = [\mu(M) - \mu(La)]/2.303RT$, it is derived from the difference between eqs. (17) and (18) as;

$$[\mu(M) - \mu(La)] = \Delta_f G^\circ(LaMO_3) - \Delta_f G^\circ(La_2O_3). \quad (19)$$

The borderline between $LaMO_3$ and $La_2Zr_2O_7$ in the presence of ZrO_2 is given as follows;

$$\mu(La) + \mu(M) + 3\mu(O) = \Delta_f G^\circ(LaMO_3) \quad (20)$$

$$2\mu(La) + 2\mu(Zr) + 7\mu(O) = \Delta_f G^\circ(La_2Zr_2O_7) \quad (21)$$

$$\mu(Zr) + 2\mu(O) = \Delta_f G^\circ(ZrO_2) \quad (22)$$

By rearranging eqs. (20) to (22), the following equation can be obtained;

$$\begin{aligned} [\mu(M) - \mu(La)] &= \Delta_f G^\circ(LaMO_3) \\ &- \Delta_f G^\circ(La_2Zr_2O_7) + 2\Delta_f G^\circ(ZrO_2). \quad (23) \end{aligned}$$

The difference between eqs. (19) and (23) corresponds to the shift of the polygonal border:

$$\begin{aligned} \Delta[\mu(M) - \mu(La)] &= \Delta_f G^\circ(La_2Zr_2O_7) \\ &- \Delta_f G^\circ(La_2O_3) - 2\Delta_f G^\circ(ZrO_2). \quad (24) \end{aligned}$$

This is the Gibbs energy change for formation of $La_2Zr_2O_7$ from ZrO_2 and La_2O_3 ; note that the difference is independent of a kind of transition metal element, M.

On the other hand, the vertical width of polygons of $LaMO_3$ (M=V,Cr,Fe) is given in a similar manner as follows;

$$\begin{aligned} \Delta[\mu(M) - \mu(La)] &= 2\Delta_f G^\circ(LaMO_3) - \\ &- \Delta_f G^\circ(La_2O_3) - \Delta_f G^\circ(M_2O_3). \quad (25) \end{aligned}$$

Since the stabilization energy of $LaMO_3$ (M=V,Cr,Fe) given in eq. (25) is much larger than that of $La_2Zr_2O_7$ in eq. (24), the Gibbs energy change for the following reaction becomes positive;



This positive value therefore suggests that transition metal perovskites would be compatible with ZrO_2 when the trivalent transition metal ions can remain unchanged.

The valence state of the transition metal ions in binary oxides however changes as a function of oxygen partial pressure. This should therefore affect the compatibility of perovskites with ZrO_2 in a similar manner to the decomposition reaction of the perovskites. For

the case of $M=V$, Fe , and Cr , the M_2O_3 phase as well as $LaMO_3$ are relatively stable over a wide range of oxygen partial pressure. In such cases, the compatibility between ZrO_2 and $LaMO_3$ is good over a wide oxygen potential range. On the other hand, for the case of $M=Ni$ and Co , the monoxide phase appears and delimits the stability polygone of perovskites; this gives rise to the high oxygen partial pressure of decomposition of perovskites as well as the high equilibrium oxygen pressure associated with the reaction between perovskites and ZrO_2 .

This effect of the lower valent oxides is represented as the following geometrical features in the chemical potential diagrams: Although the borderline of $LaMO_3$ with M_2O_3 is horizontal, borderlines with the lower valent oxides have slopes. Roughly speaking, the intersect between one of those lines and the horizontal line with La_2O_3 determines the decomposition point of the perovskite. This means that with increasing stability of the lower valent oxides, the decomposition oxygen partial pressure of perovskite increases.

As described above, the La_2ZrO_7 formation gives rise to the shift of the La_2O_3 -side border of the perovskite. Although this shift is in the same magnitude in the vertical direction, the resulting changes of the decomposition oxygen pressure are different; this is due to the deference in the geometrical features among perovskites and transition metal binary oxides. Again, the change in the equilibrium oxygen pressure becomes significant with increasing stability of the lower valent oxides.

When the divalent ions become relatively stable in the end of the transition metal series, another interesting feature appears in the reactions between $LaMO_3$ and ZrO_2 , that is, the formation of La_2ZrMO_6 ($M=Ni$) observed by Echigoya et al.²⁶⁾ This implies that a series of pseudoternary compounds, $La_{n+1}M_mZr_{n-m}$

O_{3n+1} (M =divalent transition metal and $2(3n+1)-3(n+1) = 2m+4(n-m)$), can be also formed. Appearance of such pseudoternary compounds makes it complicated to graphically show phase relations in the present type of chemical potential diagram. They also found an interesting phenomenon that reaction products between $La(Ni,Co)O_3$ and YSZ formed a multilayered reaction zone. These make it necessary to construct another type of the chemical potential diagram, a $\log \{a(La)/a(Zr)\}$ vs. $\log \{a(M)/a(Zr)\}$ plot, which was found to be effective in clarifying phase relations including the pseudoternary compounds; this also made clear correlation between the geometrical configuration of compounds in the diagram and the multilayered stacking of reaction products. This will be published elsewhere.

Since the tetravalent ions can exist in the lanthanum manganites, the A-site nonstoichiometry becomes significant. This gives rise to another feature of reaction between $LaMO_3$ and ZrO_2 ; that is, this reaction which is originated from the A-site nonstoichiometry is not accompanied with reduction of transition metal ions nor with precipitation of other transition metal oxides. As described above, the present chemical potential diagram can account for this feature reasonably from the thermodynamic point of view.

6. CONCLUSION

The present superimposed chemical potential diagrams for the La-Zr-M-O systems are quite convenient to see the stability of double oxides in the La-M-O systems and their compatibility with ZrO_2 . Since the geometrical features of the chemical potential diagram are not significantly affected by the nonstoichiometric properties, this makes it possible to construct a diagram under a stoichiometric approximation and to use it in making chemical thermodynamic considerations on phase relations with-

out losing the essential points which should be described in terms of chemical potentials.

REFERENCES

- 1) Industrial Use of Thermodynamic Data, (Ed. T. I. Barry), The Chemical Society (1980).
- 2) Application of Phase Diagrams in Metallurgy and Ceramics, (Ed. G. C. Carter), NBS Special Publication 496, NBS (1978).
- 3) User Application of Phase Diagram, Proc. an International Conference on User Applications of Alloy Phase Diagrams, (Ed. L. Kaufman), ASM international (1987).
- 4) G. Eriksson, *Chemica Scripta*, **8**, 100 (1975).
- 5) P. J. Spencer ed. CALPHAD, **7**(2), Gunnar Eriksson Special Issue (1983).
- 6) H. Yokokawa, M. Fujishige, S. Ujife and M. Dokiya, *J. Natl. Chem. Lab. Indust.*, **83**, Special Issue 1 (1988) and references therein.
- 7) H. L. Lukas, J. Weiss and E. -Th. Henig, *CALPHAD*, **6**, 229 (1982).
- 8) Bo Sundman, Bo Jansson and Jan-Olof Andersson, *CALPHAD*, **9**, 153 (1985).
- 9) H. C. Helgeson, *Pure & Appl. Chem.*, **57**, 31 (1985).
- 10) R. M. Garrels, *Diagrams of Chemical and Electrochemical Equilibria Their Setting-up and Applications*, (Ed. M. Pourbaix and A. Pourbaix), CEBELCOR, Brussels, p. 247 (1981).
- 11) H. Yokokawa, T. Kawada and M. Dokiya, *Denki Kagaku*, **56**, 751(1988).
- 12) H. Yokokawa, N. Sakai, T. Kawada and M. Dokiya, *J. Electrochem. Soc.*, **137**, 388 (1990).
- 13) H. Yokokawa, T. Kawada and M. Dokiya, *J. Am. Ceram. Soc.*, **72**, 2104 (1989).
- 14) H. Yokokawa, N. Sakai, T. Kawada, M. Dokiya, S. Kato and K. Ota, *Denki Kagaku*, **58**, 57 (1990).
- 15) H. Yokokawa, N. Sakai, T. Kawada and M. Dokiya, *Denki Kagaku*, **58**(4), (1990).
- 16) H. Yokokawa, *Kagakukogyo*, **40**, 1006 (1989).
- 17) M. Dokiya, N. Sakai, T. Kawada, H. Yokokawa, T. Iwata and M. Mori, Proc. the first international conference on solid oxide fuel cell, (Ed. S. C. Singhal), The Electrochemical Soc., Pennington p. 325 (1989).
- 18) Second Generation High Efficiency Generation System Using Coal Gas, Solid Oxide Fuel Cell Section, Investigation under Moonlight Project by MITI, Society of Japanese Machinery Industry, (1988).
- 19) B.C.H. Steele, *Ceramic Electrochemical Reactors Current Status and Application*. Ceramionics, London, (1987).
- 20) H. Yokokawa, N.Sakai, T. Kawada and M. Dokiya, *Denki Kagaku*, **57**, 821 (1989).
- 21) H. Yokokawa, unpublished work 1990.
- 22) H. Yokokawa, N.Sakai, T. Kawada and M. Dokiya, *Denki Kagaku*, **57**, 829 (1989).
- 23) C. S. Tedmon, Jr., H. S. Spacil and S. P. Mitoff, *J. Electrochem. Soc.*, **116**, 1170 (1969).
- 24) O. Yamamoto, Y. Takeda, R. Kanno and M. Noda, *Solid State Ionics*, **22**, 241 (1987).
- 25) R. Hayami and T. Yabuki, *Bull. Government Industrial Research Institute, Osaka*, **28**, 98 (1977).
- 26) J. Echigoya, S. Hiratsuka and H. Suto, *Mater. Trans. JIM*, **30**, 789 (1989).
- 27) R. Berjoan, J. P. Traverse and J. P. Coutures, *Rev. Chim. Minerale*, **10**, 309 (1973).
- 28) B. C. Tofield and W. R. Scott, *J. Solid State Chem.*, **10**, 183 (1974).
- 29) J. Shimoyama, J. Mizusaki and K. Fueki, 53 fall meeting of the Chemical Society of Japan, p. 263 (1986).